



# Characterization of the Microstructure and Thermomechanical Properties of Invar 36 Coatings Deposited by HVOF and Cold Gas Processes

W. Tillmann<sup>1</sup> · O. Khalil<sup>1</sup> · I. Baumann<sup>1</sup>

Submitted: 23 March 2022 / in revised form: 4 July 2022 / Accepted: 9 August 2022 / Published online: 31 August 2022  
© The Author(s) 2022

**Abstract** The effect of impact velocity and temperature of invar particles deposited by high-velocity oxygen fuel (HVOF) and cold spray processes on the microstructure and oxidation content of invar coatings is not fully understood. Additionally, the effect of coating thickness on the coefficient of thermal expansion (CTE) of the coated material and the influence of cold working on the coating hardness are also insufficiently investigated. In the present study, invar coatings were deposited at temperatures close to and below the melting point of invar particles to maintain low CTE. It was found that particle impact temperature and velocity strongly affect pore formation and cohesiveness but slightly affect the hardness of invar coatings. Higher particle impact velocities with impact temperatures close to the invar's melting point enhance highly the cohesiveness of HVOF-invar coatings. Furthermore, invar coatings stabilize the CTE of the coated material up to a temperature of 227 °C. An increment in the coating's thickness of 150 μm leads to reducing the CTE of the coated material (Al) in the in-plane direction by 7.65%. Applying cold working using 200 kN compression increases the hardness of the treated coatings by 6% while machine hammer peening (MHP) has a slight effect.

**Keywords** cold spray (CS) · coefficient of thermal expansion (CTE) · high-velocity oxygen-fuel (HVOF) · invar effect · machine hammer peening (MHP) · microhardness

## Introduction

Invar 36 alloy with a composition of about 36 wt.% Ni and 64 wt.% Fe is characterized by an extremely low coefficient of thermal expansion (CTE) over a wide temperature range (Ref 1-4). In 1897 Guillaume (Ref 5) discovered that face-centered cubic (FCC) alloys of iron and nickel with a nickel concentration of around 35 atomic percent exhibit anomalously low (almost zero) thermal expansion at low temperatures (between – 32 and 275 °C). This phenomenon, known as the Invar effect, makes physical properties of Invar systems, such as atomic volume, elastic modulus, heat capacity, magnetization, and Curie temperature, show anomalous behavior (Ref 6, 7). Additionally, invar 36 alloy is thermally stable below 500 °C and has good resistance to stress corrosion in the circumstance of air, seawater, and freshwater (Ref 8, 9).

Invar 36 is the metal of choice for low thermal expansion applications for many years. Owing to the very low thermal expansion coefficient, the invar 36 presents high dimensional and structural stability at varying service temperatures. Thus, the design of many precision instruments, aero-structural components, and optical parts relies on the invar 36 alloy. Furthermore, invar 36 is ideal for applications where high-dimensional stability is required over atmospheric temperature ranges, such as autoclave tooling applications. A low CTE feature is fundamental in avoiding component distortion, particularly for large components. Invar alloy also has been widely used in cryogenic liquid storage such as Liquefied Natural Gas (LNG) carriers and molds for aircraft (Ref 10-14). Additionally, metallic components, e.g., joints or mounts, that must meet the condition of very low CTE, are usually manufactured out of the invar alloy, replacing glass-ceramics (Ref 15). However, invar 36 alloy exhibits low

✉ O. Khalil  
omar.khalil@tu-dortmund.de

<sup>1</sup> Institute of Materials Engineering, Technische Universität Dortmund, Dortmund, Germany

strength and hardness, as well as poor machinability, which restricts its further use in many applications (Ref 16–18).

Many researchers have indicated that alloy element additives, such as C, Mn, Cu, Cr, Ti, and Al, can improve the strength and hardness of the invar alloys; however, the simultaneous increment in the CTE is inevitable (Ref 5, 19–23). With the development of industrial techniques, it has become a challenge to meet the fast-growing requirement of multiple industrial fields because of the bottleneck caused by the low mechanical strength of invar 36. The standard invar 36 exhibits a hardness as low as 120 HV for a CTE of  $1.2 \times 10^{-6}/^{\circ}\text{C}$  (or 1.2 ppm), while the cold working of the invar material can increase the hardness to about 260 HV. Nevertheless, the cold working hardness is considered insufficient for many applications such as tooling applications where higher hardness is required to minimize tool surface damage during handling and reduce repair and maintenance costs (Ref 24).

Since the properties of thermally- and cold-sprayed deposits are often considerably different from those of the bulk material, it is necessary to assess the relationships between spray processes and relevant process parameters on one hand and the CTE and hardness of the invar coatings on the other hand. Gibbons and Wimpenny (Ref 25) have deposited invar powders on steel substrates using the high-velocity oxygen-fuel (HVOF), and arc wire spraying (in atmospheric air and inert gas environment) processes. From the hardness perspective, invar coatings prepared by arc wire spray (in air environment) and HVOF processes offer higher hardness levels than the hardness offered by bulk Invar (250 and 140 HV; respectively). The coating prepared by air-environment arc-spray, being the most economical process, has superior hardness because of the high content of oxides. From the CTE perspective, air-environment arc-spray invar coating has relatively high CTE, about 5.7 ppm, which is significantly higher than it would be required for dimensionally stable tooling materials. In contrast, HVOF Invar coating offers relatively low CTE (in the range of 2.8–3.5 ppm), which is acceptable but deemed insufficient. Both types of coatings (prepared using arc-spray and HVOF processes) have almost the same composition, however, the nature of the air-environment arc-spray process dictates higher oxidation levels during the deposition process than that in the HVOF process. Since the CTE and hardness of invar material are directly proportional to the oxide content in the deposition, the CTE and hardness of arc-spray coatings are significantly higher than that of HVOF coatings. The authors also reported that the oxide level and hardness of the invar coatings are within certain limits influenced by the process parameters, but are significantly affected by the employed hardware.

In (Ref 26), TiC-Fe36Ni cermet coatings were synthesized by reactive plasma spraying (RPS) to increase the

hardness, in which sucrose was used as a source of carbon and as well as a binder to bind reactive constituent particles (Ti-Fe-Ni-C). The produced cermet coatings exhibited high surface hardness (about  $90 \pm 2$ , HR15N) and high microhardness (about 1640 HV<sub>0.2</sub>, Vickers Hardness), however, the authors did not refer to any CTE measurements.

Chen et al. (Ref 27) have investigated the effect of CS process parameters on the microstructure of invar coatings as well as the influence of heat treatment on the CTE. They reported that higher working gas pressure of N<sub>2</sub> or using helium (He) instead of N<sub>2</sub> have produced near fully dense structures. They also found that invar coatings before and after heat treatment showed comparable CTE values.

As an effective additive manufacturing technique, the cold gas spray (CS) process is attracting increasing interest in the last years for its high-quality metals and alloys coatings (Ref 28). In the CS process, the particles are propelled by a pressurized gas flow (nitrogen (N<sub>2</sub>) or helium) with temperatures lower than 1100 °C through a De Laval nozzle (Ref 29). The accelerated particles experience a velocity in the range of 500 to 1200 m/s while maintaining the solid-state (Ref 30, 31); hence, feedstock particles are sprayed in a solid state at low temperatures and very high velocities. Unlike conventional thermal spray processes, these unique features of CS can effectively avoid oxidation, phase change, grain growth, and cracks induced by thermal stresses (Ref 32). Additionally, the high deposition rate of CS can have a significant production level as high as 45 kg/h without size limitations (Ref 30, 33). Nowadays, the CS process is widely used to fabricate various metallic components such as pure Cu (Ref 34), Al alloys (Ref 35), pure nickel and Inconel superalloy (Ref 36), high entropy alloy (Ref 37), and metal matrix composites (Ref 38, 39).

To the authors' knowledge, the investigations on the effect of process parameters (HVOF and CS processes) as well as the effects of cold working processes on the microstructure and hardness of invar coatings are not so far adequately revealed. This study is aimed to improve the understanding of the effects of particle impact temperature and velocity and cold working post-treatment on the invar coatings. The investigations also include the influence of invar coating thickness on the thermal expansion of the coated material. In the present work, invar 36 coatings were fabricated using HVOF and cold gas (CS) techniques followed by applying cold working post-treatment processes to increase the hardness. For the HVOF process, nitrogen (N<sub>2</sub>) was injected into the combustion chamber to lower the flame temperature and increase the impact velocity of the deposited particles. Coatings microstructure was investigated and hardness measurements were performed before and after each post-treatment process. Since no oxidation process is involved in the post-treatment

processes on the investigated coatings, it is assumed that the CTE is maintained as low as that of the as-sprayed ones. Additionally, CTE measurements were performed on CS samples of different coating thicknesses (as-sprayed coatings bonded to Al substrates). The measurements were applied in the in-plane direction to investigate the effect of invar coating thickness on the CTE of the base material.

## Materials, Methods, and Processes

A commercially available invar 36 powder (hollow spherical powder (HOSP), 1.3912, supplied by Rosswag, Pfinztal, Germany) was used for the deposition of invar coatings employing HVOF and CS processes. The as-received powder was analyzed for particle size distribution using a particle size analysis instrument (S3500 Laser Diffraction, Microtrac GmbH, Germany). The utilized powder has a size distribution between 10 and 45  $\mu\text{m}$ , near-spherical morphology, with  $D_{10} = 17.0 \mu\text{m}$ ,  $D_{50} = 36.59 \mu\text{m}$ ,  $D_{90} = 47.47 \mu\text{m}$ . Table 1 summarizes the chemical composition of the utilized invar powder.

The morphology and particle size distribution of the feedstock powder is shown in Fig. 1. The high magnification image (inset image) reveals the grain structure and crystallization of the melt due to rapid solidification during the production process. It can be seen that some of the particles have satellites (particles of smaller sizes located at their surfaces), which is typical for the gas-atomized powders. Round steel and aluminum substrates, with a diameter of 40 mm and a thickness of 5 mm, were grit-blasted on one side and cleaned for coating deposition. HVOF system (Computerized Carbide Jet System, Thermico C-CJS, Japan) and a high-pressure cold spray system (Impact innovations GmbH, Germany) with a cold spray gun “Impact 5/11”, in which nitrogen ( $\text{N}_2$ ) is the working gas, were used to deposit invar 36 coatings on the prepared steel and Al substrates; respectively.

For the HVOF process, 8 experiments were conducted where all process parameters were kept constant while changing the flow rate of the  $\text{N}_2$  to vary the inflight characteristics of the invar particles. The flow rate of  $\text{N}_2$  gas was increased systematically from 0 l/min. (sample no. 1) to 350 l/min. (sample no. 8) in steps of 50 l/min. The used parameter settings are summarized in Table 2. Impact

particle characteristics (particle temperature  $P_T$  and velocity  $P_V$ ) were recorded employing an online measuring device (AccuraSpray-G3, TECNAR Automation Ltd., Qc, Canada). The produced coatings show thicknesses between 50 and 110  $\mu\text{m}$  for 10 spray overruns. Polished cross-sections from as-sprayed coatings were prepared and a series of scanning electron microscope (SEM) images were captured using a Field Emission Scanning Electron Microscope ((FESEM, JSM-7001F, Jeol, Japan).

Great attention has been paid during sample preparation (metallography) and SEM image capturing (such as settings of contrast and brightness, accelerating voltage, and probe current) to avoid the influence of sample preparation and image taking on the microstructure and evaluation of porosity and oxidation. The SEM images were analyzed utilizing Image Analysis (IA) software (ImageJ ver. 1.53 h, National Institutes of Health, Bethesda, Maryland, USA) to investigate the coating microstructure and distinguish between pores, cracks, and oxidation zones. A second HVOF experiment series was performed to produce thick invar-36 coatings (thickness range of 700–900  $\mu\text{m}$ ), in which the standoff distance was reduced by 50 mm (from 300 mm for the first 8 experiments to 250 mm), and the number of spray overruns was increased at an  $\text{N}_2$  flow rate of 150 l/min. All other process parameters were kept constant. Samples of these thick coatings were subjected to cold working (compression and MHP) post-treatment processes.

For the CS process, two types of coatings were prepared; (1) at gas pressure 3 MPa, and (2) gas pressure 5 MPa—both at gas temperature 600  $^\circ\text{C}$ —annotated as CGS-603, and CGS-605; respectively. Very thick coatings from type 1 and type 2 (thickness of 2.55 mm and 2.7 mm; respectively) were produced for the CTE measurements. Another set of CS thick coatings (thickness of 750  $\mu\text{m}$  to 950  $\mu\text{m}$ ) were prepared to investigate the effect of post-treatment processes (compression and MHP) on the microstructure and hardness. Particle impact velocities were determined using a model simulation that is based on the type, temperature, and pressure of the working gas (Ref 40). Table 2 summarizes the spray parameters that were used for both processes.

## Cold Working Post-treatment Processes

Compression and machine hammer peening (MHP) processes were applied on samples of the produced invar coatings to investigate the influence of these processes on the coating microstructure and hardness. It has been found that the application of compression and MHP results in an improvement in the microstructure and mechanical properties of additively manufactured workpieces (Ref 41), e.g., in the mold-making industry. These post-treatments

**Table 1** The chemical composition of the utilized invar powder in weight percentage (wt.%)

Ni	Cr	Mn	Si	C	Fe
35.0–37.0	< 0.50	< 0.50	< 0.50	< 0.50	Balance

**Fig. 1** size distribution and surface morphology of the used invar 36 (HOSP) powder

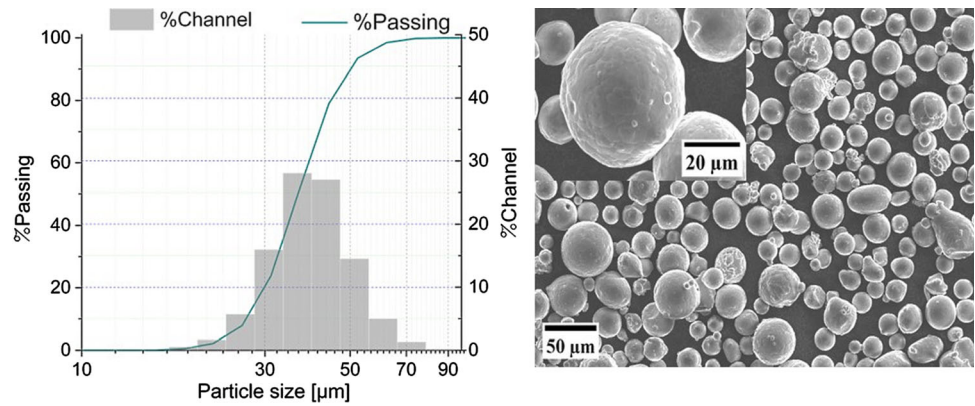


**Table 2** Utilized deposition parameters for the HVOF and CS coatings

HVOF process					
Sample annotation	Kerosene, l/min	Oxygen, l/min	Hydrogen, l/min	Standoff distance, mm	N <sub>2</sub> , l/min
Inv-1-Inv-8	12	600	60	300	0,50,...,350
Inv-150 (thick coatings)	12	600	60	250	150
Cold spray process (CS)					
Sample annotation	Gas pressure, MPa	Gas temperature, °C	Standoff distance, mm	Pass step, mm	
CGS-603	3	600	30	2	
CGS-605	5	600	30	2	

normally introduce compressive residual stresses to the coatings while reducing coating porosity and surface roughness.

*Compression/Compacting Process*

As-sprayed samples, from HVOF- and CS-coatings, were compressed at room temperature using a servohydraulic dynamic testing system (model 8802, Instron Ltd., High Wycombe, UK). The process was performed by applying an oscillated compression load (min. 5 kN to max. 200 kN) in form of a sinusoidal profile for 5 s. The applied sine profile was uniform with very low load fluctuation. After placing the sample on the fixture and fixed on the clamp, a pressing tool was applied vertically from the top and at the center of the sample, see Fig. 2. Cross-sections for the pressed zones were prepared for SEM analysis and hardness test. Additionally, hardness measurements were performed at the surface of the pressed zones.

*Machine Hammer Peening Process (MHP)*

The MHP process was carried out with a FORGEFix Air Tool by 3S engineering equipped with a carbide ball tip

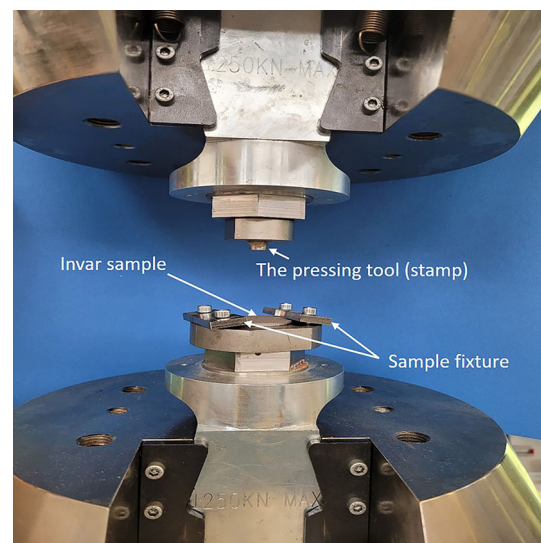


**Fig. 2** A sample of invar coating sprayed on a steel substrate is prepared for an oscillated compression load

with a diameter of  $d_p = 16$  mm mounted in a 5-axis computerized numerical control (CNC) machining center Deckel Maho DMU 50 eVolution. Samples of invar coatings (HVOF & CS) were subjected to the MHP process at

room temperature with varied process parameter settings in three locations for the same sample as can be seen in Fig. 3. The varied process parameters are maximal indentation depth ' $a_{i,max}$ ', feed velocity ' $v$ ', and track distance ' $l_p$ '. In all settings, the MHP tool was working with a hammering frequency ' $f$ ' of about 200 Hz. The NC path used for NC processing was always oriented in the radial direction of the samples. The compressed air pressure used to power the MHP tool was kept constant at ' $p$ ' = 6 bar during all experiments to achieve the maximum possible impact energy and, thus, maximum coating compaction.

### Thermal Expansion Test (CTE)

Composite samples of thick Invar coatings, cold-sprayed on Al substrates, were used to perform CTE measurements from room temperature (RT) to 300 °C using horizontal differential dilatometer with Quartz sample holder and single push rod (DIL L75 LT, Linseis messgeräte GmbH, Selb, Germany). The measurements were performed on the samples in the “in-plane” direction, that is, along the diameter of the round sample. Therefore, cylindrical rods of 20 mm length and 4 mm diameter were machined from the composite samples. The cylindrical rod of the composite sample consists of Al substrate in the lower half and invar 36 coating in the upper half. A freestanding Al substrate was machined the same way and subjected to the same measurement. The measurements were performed in atmospheric air, which explains the dark color of the invar coatings after measurement completion. The change in sample length ( $\Delta L$ ,  $\mu\text{m}$ ) was recorded during the heating process at a precision of 0.05  $\mu\text{m}$ . The coefficient of thermal expansion (CTE,  $\mu\text{m}/\text{m} \cdot ^\circ\text{C}^{-1}$ ) is then calculated according to the equation  $\text{CTE} = \Delta L / (\Delta T \cdot L_0)$ , where ( $\Delta T$ ,  $^\circ\text{C}$ ) is the temperature difference, and ( $L_0$ , m) is the sample initial length at room temperature. Figure 4 shows images for the different samples with their dimensions that were subjected to CTE measurements.

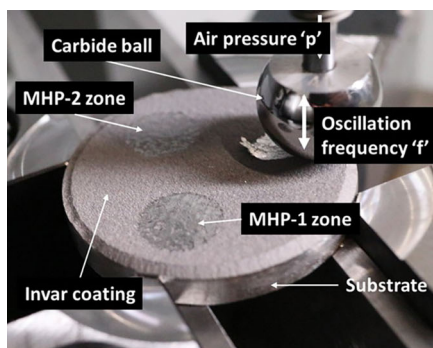


**Fig. 3** MHP post-treatment applied on an invar coating sample with three different process settings

### Hardness Test

Polished cross-sections of invar-36 samples, prepared by both processes (HVOF and CS), were subjected to hardness measurements (Vickers, HV0.3) at room temperature, using a Vickers microindenter (Duramin-40 A1, Struers GmbH, Maassluis, Netherlands). The test was applied on invar samples in as-sprayed conditions and after applying cold working post-processes (compression, and MHP). The average hardness value was calculated from five random indentations in each sample. The indentations were performed with a load of 2.94 N for a dwell time of 15 s. Standard spacing was used between the indentations (at least three times the diagonal) to ensure that no further stresses were produced by the interaction between the consecutive indentations.

## Results and Discussion

### Effect of Varying $N_2$ Flow Rate on Inflight Particle Characteristics, Microstructure, and Oxidation Level of Invar-36 Coatings Prepared by HVOF Process

From Fig. 5, the effect of varying the  $N_2$  flow rate on the particle impact temperature ( $P_T$ ) and velocity ( $P_V$ ) is obvious. Higher  $N_2$  flow rates lead to higher levels of gas expansion inside the combustion chamber, and consequently to increasing particle velocities. At the same time,  $N_2$  as an inert gas does not contribute to the combustion process. As a result, the heat capacity within the chamber increases, which reduces the temperature of the flame and accelerates particles. Therefore,  $P_T$  is decreased continuously as the flow rate of  $N_2$  is increased. From the  $P_T$  curve, it can be seen that the decrement rate is almost regular and becomes higher when the flow rate of nitrogen exceeds 150 l/min. On average, the decrement rate of  $P_T$  is about 1 K per 1 l/min increment in nitrogen flow. In contrast,

*The applied MHP parameter settings*

MHP setting	Max. indent. depth [ $a_{i,max}$ , mm]	Feed velocity [ $v$ , mm/min]	Track dist. [ $l_p$ , mm]
MHP-1	0.20	2000	0.15
MHP-2	0.30	1000	0.05
MHP-3	0.45	1000	0.05

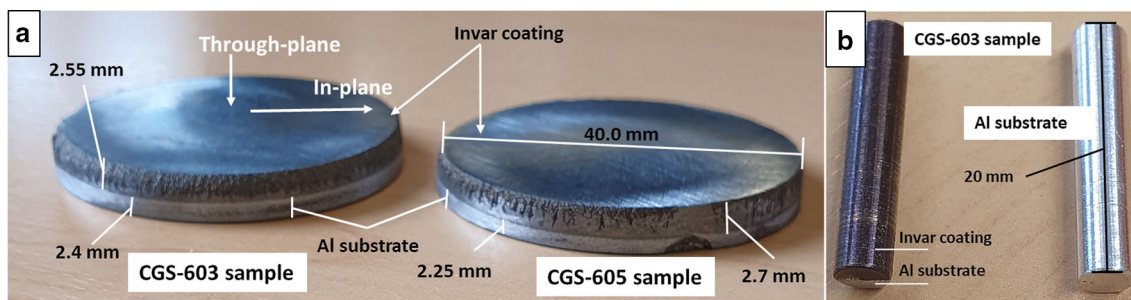
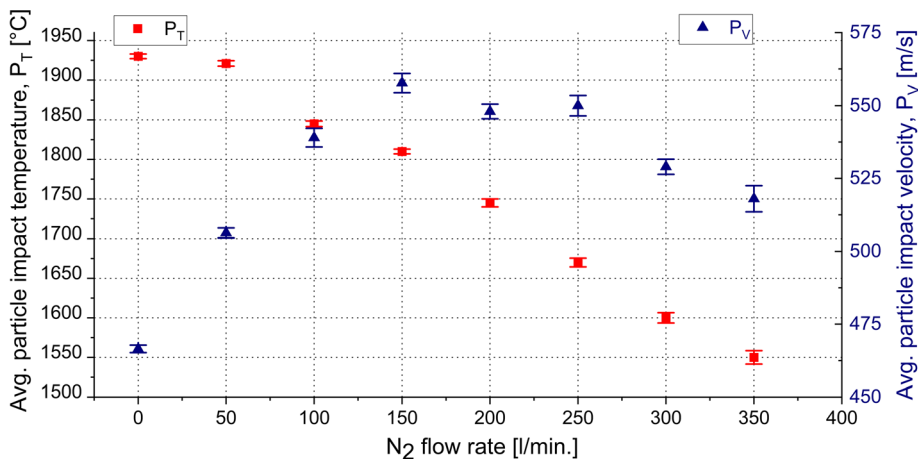


**Fig. 4** (a) Invar-36 coating sprayed by CS on Aluminum substrate at different gas pressures, (b) composite (CGS-603), and freestanding Al substrate samples that were used for CTE measurement

**Fig. 5** Effect of varying  $N_2$  flow rate on invar particle impact temperature and velocity—HVOF process. The error bars represent the standard deviation of the measurements



particle impact velocity ( $P_V$ ) is increased linearly when the nitrogen flow rate is increased from 0 to 150 l/min. Further increment in the nitrogen flow rate beyond 150 l/min stabilizes  $P_V$  at about 550 m/s. For nitrogen flow rates higher than 250 l/min,  $P_V$  decreases with a rate of about 3.5 m/s per 10 l/min increments in the nitrogen flow rate. It can be observed that increasing the  $N_2$  flow rate beyond 150 l/min further decreases the temperature of flame and  $P_T$ , and eventually, the  $P_V$ .

As a result of the varied  $P_T$  &  $P_V$ , the microstructure of the formed invar coatings shows different appearances. At relatively low  $P_V$  and high  $P_T$ , the cross-section of the coatings exhibits an incoherent structure with coarse pores and detached splats. Low particle impact velocities lead to a relatively low degree of particle deformation upon impact on the substrate surface or the underlying layer. As a result, weak mechanical interlocking between the deposited splats and pore formation between the sequential splats occurred. Thick oxide films (annotated by white arrows in Fig. 6a, b, and c) that surround the splats indicate high levels of oxidation. Oxides are easily distinguished from pores and cracks in SEM images as they exhibit brighter gray levels. When impact  $P_V$  is increased with a simultaneous decrease in impact  $P_T$  (but still considerably higher than the melting point of invar-36, which is  $\approx 1690$  °C), cross-sections

show a consistent and coherent structure as a result of improved interlocking between the deposited splats. In addition, oxide films at the splats boundaries are observed to become thinner, see Fig. 6d. When impact  $P_T$  decreases approaching the melting point of the invar, the cross-sections show a dense crack network and poor adhesion with the substrate despite relatively high impact  $P_V$ . However, only a few thin oxide films at the splats boundaries are observed due to high impact  $P_V$ , see Fig. 6(e), and (f). Under the experimental setup of the present work and relevant results, invar coating prepared at 150 l/min nitrogen flow rate ( $P_T = 1810$  °C and  $P_V = 560$  m/s) has shown good coating microstructures in terms of coating cohesiveness, low oxide content, and coating/substrate adhesion. Figure 6 shows cross-sections of invar-36 coatings that were produced at different impact  $P_T$  and  $P_V$  by adjusting the rate of nitrogen flow.

**Effect of Cold Gas Spraying (CS) Process Parameters on the Microstructure of Invar Coatings**

From Fig. 7(a), and (b), it can be seen that the invar coating deposited at 5 MPa gas pressure (Fig. 7b) is denser (possessing lower amounts of pores) than the coating deposited at 3 MPa. The higher pressure leads effectively to a higher

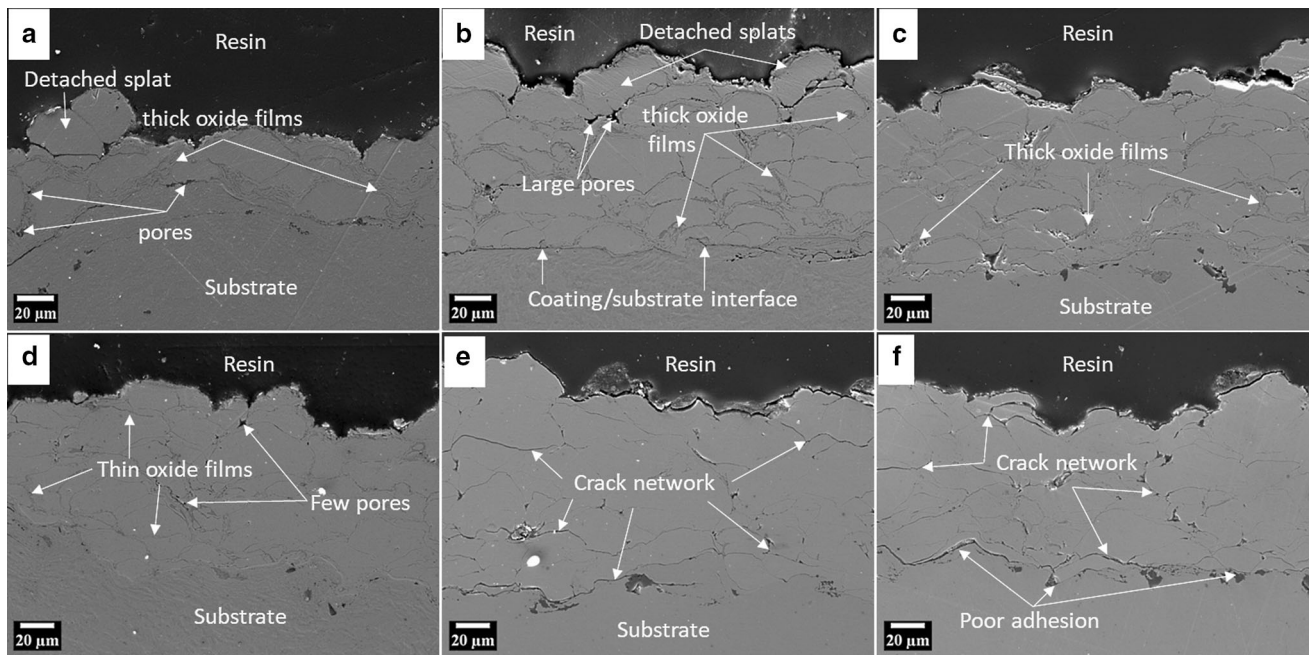
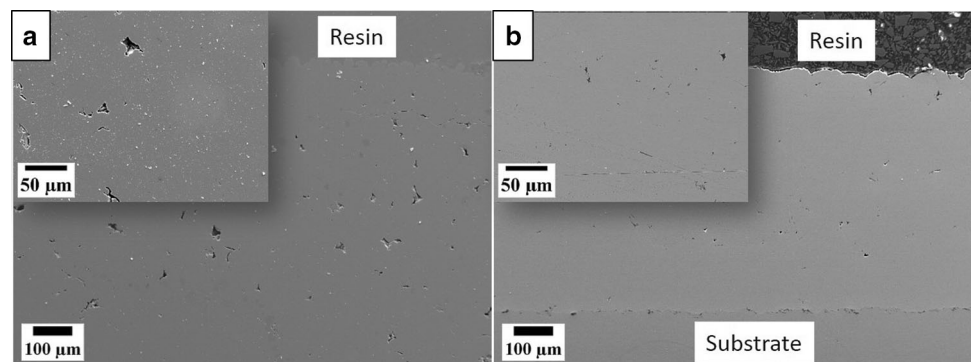


**Fig. 6** SEM images showing the microstructure and oxidation level of invar-36 coatings at nitrogen flow rates (a) 0 l/min, (b) 50 l/min, (c) 100 l/min, (d) 150 l/min, (e) 200 l/min, and (f) 300 l/min

**Fig. 7** Cross-sectional SEM images of invar coatings cold-sprayed at working gas pressure of (a) 3 MPa, and (b) 5 MPa



impact velocity of inflight the particles. From the model simulation (39), impact velocities for invar particles are estimated as 680 and 725 m/s at 3 MPa and 5 MPa; respectively. Porosity measurements show that the coating deposited at 680 m/s possesses 1.2% porosity on average against only 0.346% porosity for coatings deposited at 725 m/s. Lower impact velocity led to forming large-sized pores and higher pore-number compared to pore size and number resulting from higher impact velocity. These results are in a well agreement with the literature data (Ref 27).

Higher impact velocities allow for sufficient particle deformation during the deposition process that leads to nearly fully dense structure and limits the generation of coarse-sized pores, therefore, only very few fine-sized pores are observed. However, SEM images at higher magnification factors show comparable oxide content

within the investigated coatings despite the difference in the impact velocity of the deposited particles. This is most likely due to the short standoff distance (30 mm) and low inflight particle temperature.

#### Thermal Expansion (CTE) Measurement of Composites of CS-Invar 36 Coating Sprayed on Al Substrates

CTE measurements were performed on samples of invar coatings cold sprayed on aluminum substrates at 3 MPa and 5 MPa gas pressures (samples CGS-603 and CGS-605) as well as on a freestanding aluminum substrate. Aluminum was selected as a base material (substrate) due to its relatively high CTE (about 23 times as CTE of invar). The measurements were performed in the direction of sample diameter (in-plane), which means that the measured

thermal expansion is the combined expansion of the coating and substrate as one component. Measuring CTE in the direction of substrate-coating (through-plane) is not relevant here as it results in the sum of individual thermal expansion for the materials that compose the sample.

### In-Plane CTE Measurement

Figure 8(a) shows a schematic diagram for the in-plane CTE measurement where the composite sample is fixed from one side and the expansion is measured at the other side. Theoretically, when the composite sample is heated up, the lower part of the sample (Al substrate) would expand more than the upper part (invar-36 coating) due to the large difference in their CTEs (free expansion for each material is denoted by dashed lines). However, because the two parts are bonded together and expand as one component, the invar coating (the part with lower expansion) will experience a tension force (pulled outwards) by the Al substrate (the part with higher expansion), which attempts to expand more. In turn, the Al substrate will experience a compression force (pulled in) by the invar-36 coating (the part with lower expansion), which attempts to expand less. Therefore, the composite sample will expand with a magnitude ( $dl_{sample}$ ) that lies between the free expansion values for the two composing parts ( $dl_{coating}$  &  $dl_{substrate}$ ). The sample expansion will depend mainly on the free expansion of the materials composing the sample and thermal stress originated by the Al substrate in form of tension force, as well as the compression force that results from the invar coating on the Al substrate. In the end, the composite sample will extend to a compromised position, resulting in an effective compression of the Al substrate from its free expansion position and an effective extension of invar coating from its free expansion position.

Figure 8(b) presents temperature-dependent CTE measurements for two CS invar coatings with different

thicknesses (2.55 & 2.7 mm) sprayed on Al substrates and a freestanding Al substrate, while Fig. 9 shows their relative thermal expansion. From Fig. 8(b), it is obvious that in the first stage (RT to 138 °C), the measured CTE values for the composite samples (22.2 and 20.5 ppm) are constant and almost equal to the thermal expansion of the freestanding Al substrate. In the second stage of evolution (138–227 °C), the CTE value of the composite sample (CGS-605) is increased slightly by about 3% against 16.6% for the freestanding Al substrate. However, the CTE value of the said composite sample is still lower than that of the other composite sample (CGS-603) and freestanding substrate. The invariability and slight increase in the CTE value for both composite samples in contrast to the linear increment of the freestanding substrate throughout this stage reveals the effect of the invar coatings on the overall CTE value.

In the third stage (227–300 °C), both composite samples show a gradual increase in their CTE values, which is analogous to that of the freestanding substrate. This increment was expected because invar-36 has almost invariable CTE only up to 227 °C, beyond that temperature, the rate of expansion increases gradually up to Curie temperature (280 °C), where the thermal expansion starts to increase linearly.

The presented CTE curves for the composite samples and standalone substrate reveal a general effect due to the invar effect (stable and extremely low CTE) of invar coating, and a specific effect of relative thicknesses of the individual materials that compose the samples.

The general effect is that the CTE of the composite samples is kept invariable (or with a very slight increment) up to temperature 227 °C. This is compared to the CTE curve of the freestanding substrate, which started to increase linearly at about 100 degrees earlier (at a temperature of 130 °C).

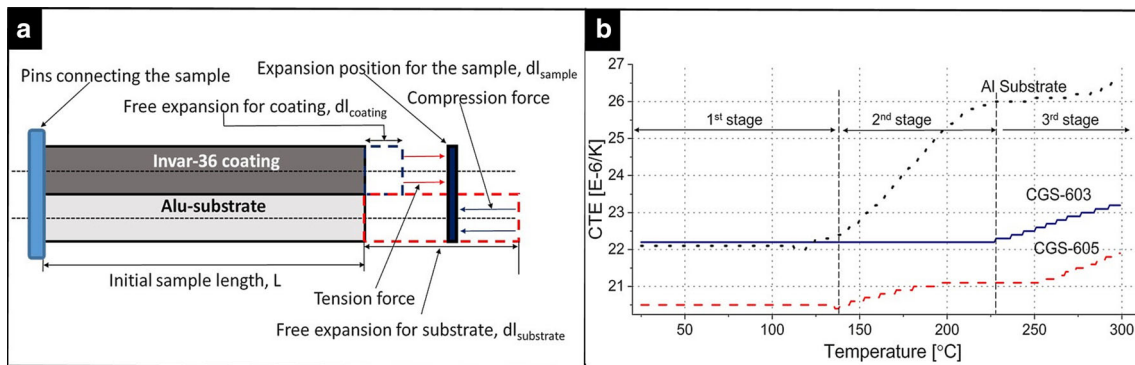
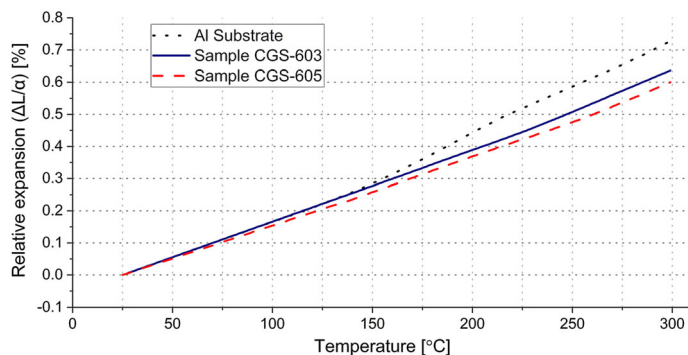


**Fig. 8** In-plane CTE measurement; (a) A schematic diagram illustrates the evolution of thermal expansion behavior for a composite sample consisting of Al substrate and cold sprayed

invar-36 coating, (b) CTE measurements for a freestanding Al substrate and two composite samples (invar coatings with different thicknesses that are cold sprayed on Al substrate)



**Fig. 9** Relative thermal expansion for freestanding Al substrate and two composite samples (invar coating cold-sprayed on Al substrate)



The specific effect of the relative thicknesses of the individual materials within the composite samples is seen obviously in the difference in the CTE values for the composite samples. The composite sample with thicker invar coating (CGS-605) shows considerably lower CTE values along the whole course of the measurement. Quantitatively, increasing thickness of the invar coating by 0.15 mm accompanied by a thickness decrement for the Al substrate by the same amount results in a reduction by 7.65% in CTE value for the composite (from 22.2 to 20.5 ppm). Providing that the relationship between the composite CTE and the individual thicknesses is linearly proportional, the CTE of the composite can be reduced by about 50% (from 23 to 11.3 ppm) if the individual thickness of the invar coating is higher than that of the Al substrate by 1.0 mm. However, the large difference in the individual thicknesses can lead to partial or complete delamination of the coating at large temperature changes due to the high CTE mismatch between invar coating and Al substrate.

Another factor that may contribute to a lower CTE value for the composite sample (CGS-605) is that it was sprayed at 5 MPa gas pressure while the other sample (CGS-603) was sprayed at 3 MPa. Higher gas pressure implies higher particle impact velocity, and consequently, higher kinetically-induced residual compressive stresses.

### Calculating Free Thermal Expansion (CTE) of Invar Coating in the In-Plane Direction

Since the invar coating and Al substrate composing the sample are still bonded (invar coating did not delaminate from the Al substrate during and after performing the measurement), the following conclusion can be stated:

$$\begin{aligned} &\text{Thermal tensile force in invar coating} \\ &= \text{Compressive force in Al substrate} \end{aligned}$$

This conclusion can be written mathematically as follows:

$$(\sigma \cdot A)_{\text{invar}} = (\sigma \cdot A)_{\text{Alsubstrate}} \quad (\text{Eq 1})$$

where “ $\sigma$ ” is the thermal/compressive stress, and “ $A$ ” is the area of the individual material composing the sample being tested for CTE.

Defining the thermal/compressive stress of each material in terms of its CTE “ $\alpha$ ”, Eq 1 can be reformulated as follows:

$$(E \cdot \alpha \cdot \Delta T \cdot A)_{\text{invar}} = (E \cdot \alpha \cdot \Delta T \cdot A)_{\text{Alsubstrate}} \quad (\text{Eq 2})$$

where “ $E$ ” is Young’s modulus, “ $\alpha$ ” is the coefficient of linear thermal expansion, and “ $\Delta T$ ” is the temperature change. Please note that Young’s modulus “ $E$ ” for bulk invar was used for the calculation of CTE.

In this case, thermal stresses for the materials that compose the sample are relatively proportional to their Young’s modulus, CTE, and individual area since they are subjected to the same temperature change “ $\Delta T$ ”.

The above equation (Eq 2) was used to find the individual contribution of invar coating ( $\alpha_{\text{invar}}$ ) to the thermal expansion of the composite sample, and the result is shown in Fig. 10.

### Effect of Post-treatment on the Microstructure and Hardness of Invar Coatings

#### Compression Process

Figure 11 shows a cross-sectional SEM image for HVOF-invar coating (the image in the middle), in which only the left half of the cross-section is compressed while the other one is still in the as-sprayed condition. The sample was partially subjected to a compression process normal to the top view plane at 200 kN. Due to the nature of the thermal spray process, the microstructure of the as-sprayed (uncompressed) part exhibits a network of cracks and oxide films as well as pores of different sizes at the boundaries of the accumulated splats. Compared to the as-sprayed cross-section, the compressed cross-section shows splats of relatively smaller sizes showing the horizontally oblate shape and thinner oxide films. It is believed that the compression process has made the coating denser as a result of the

**Fig. 10** Individual contribution to the CTE (mathematically calculated) of cold-sprayed invar coating produced using 5 MPa gas pressure on Al substrate in the in-plane direction showing the same CTE curve for bulk invar 36

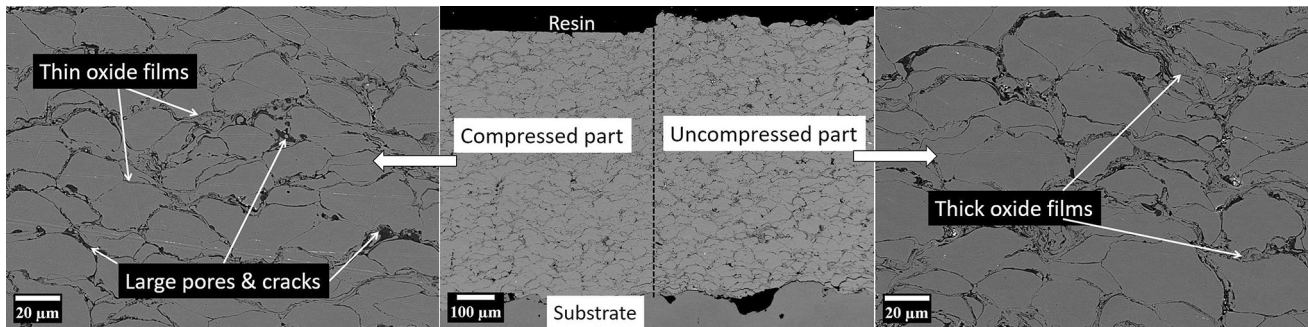
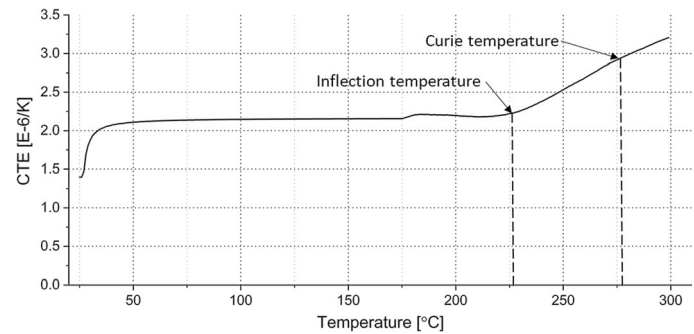


**Fig. 11** Cross-sectional SEM images for HVOF invar coatings showing the effect of compression process on the microstructure: (middle) compressed and as-sprayed parts of the coating, (left) compressed part of the coating, (right) as-sprayed part of the coating

healing of the fine pores and cracks as well as due to the thinning of oxide films. The process was not sufficient to make large pores and cracks vanish due to their coarse size and morphology. Pores and cracks are easily distinguished from oxide films by their relatively darker grey level.

According to the present work setup, the applied compression process had the effect to decrease the coating thickness by about 6% on average (about 50  $\mu\text{m}$ ) and increase the hardness by about 6% (from 248 to 263 HV0.3).

In contrast to the HVOF-invar coating, the compressed CS-invar coating appears the same as the as-sprayed coating except it shows a nearly full dense structure with a rare existence of pores. The nature of the CS process results in a very dense coating structure, which allows very low margins for further densification. Therefore, the hardness test for the compressed CS-coating reveals a very low increment in the hardness compared to the as-sprayed one (from 245 to 253 HV0.3). For both types of invar coatings, the applied compression process affected only the upper half of the coating.

#### *Machine Hammer Peening (MHP) Process*

Compared to the compression process, the MHP process affected only the surface layer to a depth of 100–150  $\mu\text{m}$  when applied to HVOF- and CS-invar coatings with no thickness reduction being observed in the treated zones.

Therefore, only the surface layer shows a fully dense structure with almost 0% porosity, see Fig. 12. Additionally, it is clearly observed that the microstructure of the invar coating is insensitive to MHP process parameters because the used MHP settings led to the same limited influence.

Hardness test on the coatings that are MHP-treated at different settings led almost to the same hardness level with a slight difference compared to that of the as-sprayed coating. Figure 13 shows images for indentations applied on as-sprayed, compressed, and MHPed invar coatings that are prepared using CS, and HVOF processes. The differences in lengths of diagonals indicate the difference in the indent depth, and consequently, the coating hardness.

From Fig. 14, it is obvious that the compression process has an advantage over the MHP process in improving the hardness of invar coatings.

## Summary and Conclusion

In the present work, invar-36 coatings were deposited on steel and Al substrates using HVOF and CS processes to investigate the effect of impact velocity and temperature of the particles (for HVOF process) and gas pressure and temperature (for CS process) on coating microstructure before (as-sprayed) and after cold working. For the HVOF process, the velocity and temperature of the impact

**Fig. 12** SEM images for (a) HVOF- and (b) CS-invar coatings, each showing as-sprayed and post-treated (MHP) cross-sections. SEM images of a high-magnification factor for the HVOF treated coating show (c) the affected and (c and d) the non-affected zones

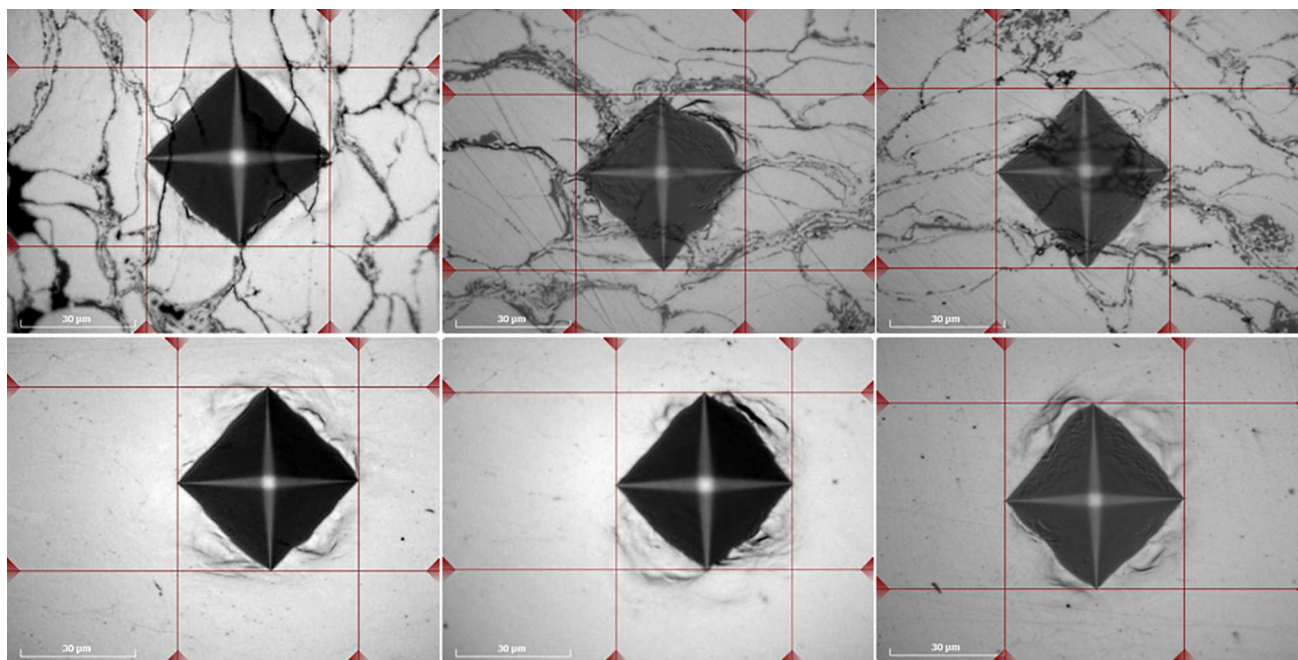
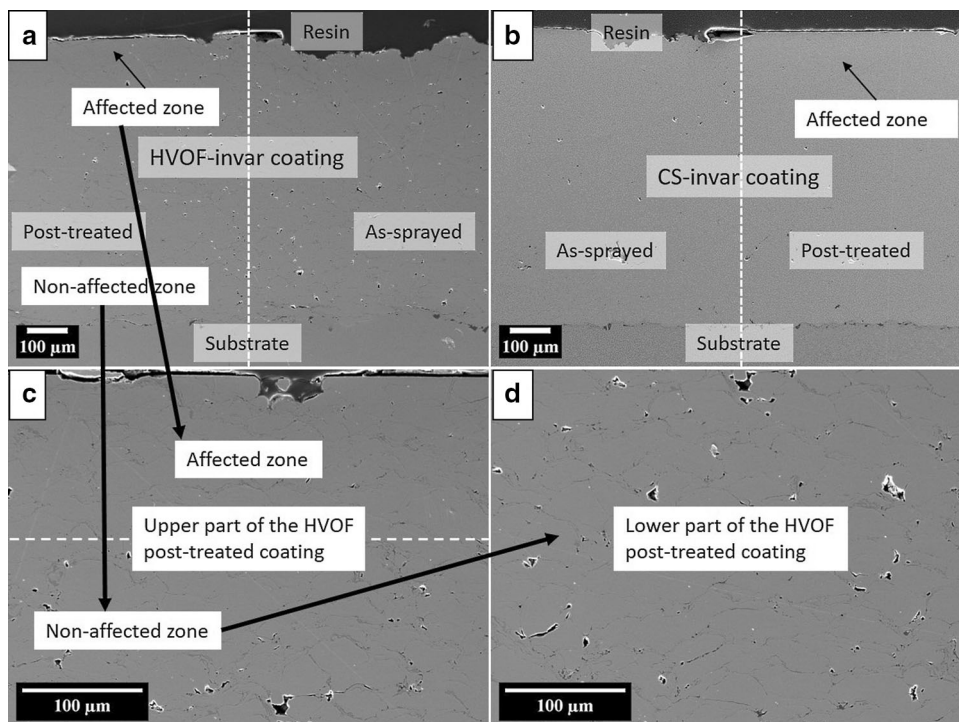


**Fig. 13** Indentations of Vickers hardness tester (HV03) in HVOF (a, b, and c), and CS (d, e, and f) invar coatings in as-sprayed, compressed, and MHPed conditions; respectively

particles were varied by systematically changing the flow rate of the nitrogen. To investigate the effect of cold working post-processes on the hardness, compression up to 200 kN and MHP with three different settings were applied on both types of invar coatings. Additionally, the coefficient of thermal expansion (CTE) for Al substrate that is

cold sprayed with invar-36 was measured in the in-plane direction from room temperature to 300 °C in atmospheric air. According to the performed measurements and obtained results from the conducted experiments, the following conclusions can be drawn:

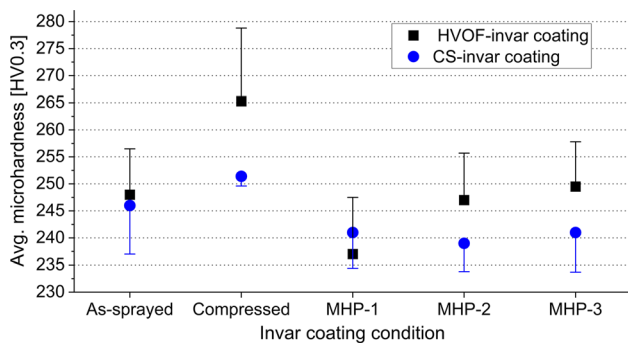


**Fig. 14** Hardness test for HVOF- and CS-invar coatings in as-sprayed and cold working conditions (standard deviation is represented by a one-sided error bar)

- Good quality HVOF-invar coating (in terms of coating cohesiveness and oxidation level) is produced at higher particle impact velocities and particle impact temperatures just above the melting temperature of the invar powder.
- For the CS process, increasing working gas pressure from 3 to 5 MPa at gas temperature 600 °C increases particle impact velocity (from 680 to 725 m/s), which leads to higher particle deformation and consequently, to a fully dense coating structure.
- Due to relatively low particle impact temperatures for the CS process (about 600 °C) in comparison to the HVOF process, CS-coatings possess very low porosity levels and almost no cracks as well as low oxide contents.
- Invar coatings stabilize the thermal expansion of the underlying material (substrate) within a wide range of temperatures (up to 227 °C) while the thickness of the invar coating plays a significant role in reducing the CTE of the coated material (7.65% reduction in the CTE for each additional 300 µm in the thickness of the invar coating).
- Applying compression process cold working post-treatment on HVOF-invar coatings densified the upper layer leading to reduced porosity and thinning of the oxide films within the affected zone while improving coating hardness.
- Similar to the compression process, MHP treated zones show almost the same effect on the microstructure of the invar coatings. Both cold working processes affect only the surface layer of the coating, however, the hardness of the treated coatings is slightly affected compared to the as-sprayed ones.

**Acknowledgments** The authors thank the Institute of Machining Technology (Institut für Spanende Fertigung, ISF, Technical University of Dortmund) for performing the MHP cold working process on the prepared invar samples. The authors also thank the

instrumentation team at Linseis Messgeräte GmbH (Selb, Germany) for machining the samples and providing the CTE measurements.

**Open Access** This article is licensed under a Creative Commons Attribution 4.0 International License, which permits use, sharing, adaptation, distribution and reproduction in any medium or format, as long as you give appropriate credit to the original author(s) and the source, provide a link to the Creative Commons licence, and indicate if changes were made. The images or other third party material in this article are included in the article's Creative Commons licence, unless indicated otherwise in a credit line to the material. If material is not included in the article's Creative Commons licence and your intended use is not permitted by statutory regulation or exceeds the permitted use, you will need to obtain permission directly from the copyright holder. To view a copy of this licence, visit <http://creativecommons.org/licenses/by/4.0/>.

**Funding** Open Access funding enabled and organized by Projekt DEAL.

## References

1. Y. Ustinovshikov and I.A. Shabanova, Study of Microstructures Responsible for the Emergence of the Invar and Permalloy Effects in Fe-Ni Alloys, *J. Alloys Compd.*, 2013, **578**, p 292-296.
2. C.V. Prică, B.V. Neamtu, F. Popa, T.F. Marinca, N. Sechel and I. Chicinas, Invar-Type Nanocrystalline Compacts Obtained by Spark Plasma Sintering from Mechanically Alloyed Powders, *J. Mater. Sci.*, 2018, **53**(18), p 3735-3743.
3. K. Nakama, S. Tatsutani, K. Sugita and Y. Shirai, Strengthening of Fe-36mass% Ni Low Thermal Expansion Alloy by Additions of C, V, Ti, and Cr and the Effect of Reducing Ni on Thermal Expansion, *J. Jpn. Inst. Met. Mater.*, 2014, **78**, p 37-44.
4. E.S. Gorkunov, A.I. Uvarov, V.M. Somova and V.A. Kazantsev, Effect of Aging and Plastic Deformation on the Mechanical, Magnetic, and Thermal Properties of Cobalt-Containing Invars, *Russ. J. Nondestruct. Test.*, 2005, **41**, p 802-808.
5. C.E. Guillaume, The Anomaly of the Nickel-Steels, *J. Frankl. Inst.*, 1919, **191**, p 374-404.
6. E.P. Wohlfarth and K.H.J. Buschow, *Ferromagnetic Materials: A Handbook on the Properties of Magnetically Ordered Substances*, Vol 5 Amsterdam, North-Holland, 1990, p 237-322
7. R.J. Weiss, The Origin of the 'Invar' Effect, *Proc. Phys. Soc.*, 1963, **82**, p 281-288.
8. H. Saito et al., *Physics and Applications of Invar Alloys*, Maruzen Co., Tokyo, 1978.
9. J.L. Zhu, J.H. Huang, H.T. Wang et al., In-situ Synthesis and Microstructure of TiC-Fe36Ni Composite Coatings by Reactive Detonation-Gun Spraying, *Mater. Lett.*, 2008, **62**(12-13), p 2009-2012.
10. G.V. Adamov, V.M. Bukhanov, J.S. Colligon, K.F. Minnebaev, A.A. Nasretidinov, L.B. Shelyakin, V.E. Yurasova and EYu. Zykova, Secondary Ion Emission of Fe-Ni alloys in the Temperature Range Including the Curie Point, *J. Vacuum*, 2004, **73**(1), p 47-52.
11. J.L. Corbacho, J.C. Suárez and F. Molleda, Grain Coarsening and Boundary Migration During Welding of Invar Fe-36Ni Alloy, *Mater. Charact.*, 1998, **41**, p 27-34.
12. S.W. Choi, J.U. Roh, M.S. Kim and W.I. Lee, Analysis of Two Main LNG CCS (Cargo Containment System) Insulation Boxes for Leakage Safety Using Experimentally Defined Thermal Properties, *Appl. Ocean Res.*, 2012, **37**, p 72-89.

13. Y. Zhao, Y.S. Sato, H. Kokawa and A.P. Wu, Microstructure and Properties of Friction Stir Welded High Strength Fe-36 wt%Ni Alloy, *Mater. Sci. Eng.*, 2011, **528**, p 7768-7773.
14. M. Inaba, Y. Honma, T. Hatanaka and Y. Otake, Effects of the Annealing Conditions on the Oxidation Behavior of Fe-36 Ni Alloy, *EAPPL. Surf. Sci.*, 1986, **27**, p 164-179.
15. J.S. Distl, H.J. Juranek and G. Luichtel, Expansion Behaviour of Superinvar in the Vicinity of Martensite Transformation Temperature, *Steel Res. Int.*, 2001, **72**(10), p 416-420.
16. J.M. Nan, G.X. Li and K.W. Xu, Yielding Behavior of Low Expansion Invar Alloy at Elevated Temperature, *J. Mater. Process. Technol.*, 2001, **114**, p 36-40.
17. L.D. Bobbio, R.A. Otis, J.P. Borgonia, R.P. Dillon, A.A. Shapiro, Z.K. Liu and A.M. Beese, Additive Manufacturing of a Functionally Graded Material from Ti-6Al-4V to Invar: Experimental Characterization and Thermodynamic Calculations, *Acta Mater.*, 2017, **127**, p 133-142.
18. M. Yakout, M.A. Elbestawi and S.C. Veldhuis, A Study of Thermal Expansion Coefficients and Microstructure During Selective Laser Melting of Invar 36 and Stainless Steel 316L, *Addit. Manuf.*, 2018, **24**, p 405-418.
19. J.F. Zhang, Y.F. Tu, J. Xu, J.S. Zhang and J.L. Zhang, Effect of Solid Solution Treatment on Microstructure of Fe-Ni Based High Strength Low Thermal Expansion Alloy, *J. Iron Steel Res. Int.*, 2008, **15**, p 75-78.
20. W. Chao, S.Q. Yuan, Z.J. Wang and Z.P. Feng, Effects of W + Nb on Thermal Expansion Property and Microhardness of Fe-Ni Invar Alloy, *Rare Metal. Mat. Eng.*, 2014, **43**, p 460-464.
21. Y.C. Yu, W.G. Chen and H.G. Zheng, Effects of Ti-Ce Refiners on Solidification Structure and Hot Ductility of Fe-36Ni Invar Alloy, *J. Rare Earth*, 2013, **31**, p 927-932.
22. S.H. Wang, J.T. Guo, W.H. Lai, Y.L. Ge, M.H. Tan and H. Li, Microstructure and Mechanical Properties of Fe-Ni-Co-Base Superalloy After Long-Term Aging at 650 °C, *Acta Metall. Sin.*, 1991, **4**, p 194-198.
23. M. Onoue, G. Trimarchi, A.J. Freeman, V. Popescu and M.R. Matsen, Magnetization of Ternary Alloys Based on Fe0.65Ni0.35 Invar with 3d Transition Metal Additions: An ab initio Study, *J. Appl. Phys.*, 2015, **117**, p 043912.
24. Anon, Nilo Alloy 36 Material Specification Sheet 3721, Company Literature, Inco Alloys International Inc., (Huntington, WV, USA, 1981)
25. G. Gibbons and D. Wimpenny, Mechanical and Thermomechanical Properties of Metal Spray Invar for Composite Forming Tooling, *J. Mater Eng Perform*, 2000, **9**, p 630-637.
26. J. Zhu et al., Microstructure and Properties of TiC-Fe36Ni Cermet Coatings by Reactive Plasma Spraying Using Sucrose as Carbonaceous Precursor, *Appl. Surf. Sci.*, 2008, **254**, p 6687-6692.
27. C. Chen et al., Cold Spray Additive Manufacturing of Invar 36 Alloy: Microstructure, Thermal Expansion and Mechanical Properties, *J. Mater. Sci. Technol.*, 2021, **72**, p 39-51.
28. W. Li, K. Yang, S. Yin, X. Yang, Y. Xu and R. Lupoi, Solid-State Additive Manufacturing and Repairing by Cold Spraying: A Review, *J. Mater. Sci. Technol.*, 2018, **34**(3), p 440-457.
29. S. Yin, M. Meyer, W. Li, H. Liao and R. Lupoi, Gas Flow, Particle Acceleration, and Heat Transfer in Cold Spray: A Review, *J. Therm. Spray Technol.*, 2016, **25**, p 874-896.
30. S. Yin, P. Cavaliere, B. Aldwell, R. Jenkins, H. Liao, W. Li and R. Lupoi, Cold Spray Additive Manufacturing and Repair: Fundamentals and Applications, *Addit. Manuf.*, 2018, **21**, p 628-650.
31. C. Lee and J. Kim, Microstructure of Kinetic Spray Coatings: A Review, *J. Therm. Spray Technol.*, 2015, **24**, p 592-610.
32. K. Yang, W. Li, X. Guo, X. Yang and Y. Xu, Characterizations and Anisotropy of Cold-Spraying Additive-Manufactured Copper Bulk, *J. Mater. Sci. Technol.*, 2018, **34**, p 1570-1579.
33. R.N. Raoelison, C. Verdy and H. Liao, Cold Gas Dynamic Spray Additive Manufacturing Today: Deposit Possibilities, Technological Solutions, and Viable Applications, *Mater. Des.*, 2017, **133**, p 266-287.
34. B. Yu, J. Tam, W. Li, H.J. Cho, J.G. Legoux, D. Poirier, J.D. Giallonardo and U. Erb, Microstructural and Bulk Properties Evolution of Cold-Sprayed Copper Coatings after Low-Temperature Annealing, *Materialia*, 2019, **7**, p 100356.
35. X. Xie, Y. Ma, C. Chen, G. Ji, C. Verdy, H. Wu, Z. Chen, S. Yuan, B. Normand, S. Yin and H. Liao, Cold Spray Additive Manufacturing of Metal Matrix Composites (MMCs) Using a Novel Nano-TiB<sub>2</sub>-Reinforced 7075Al Powder, *J. Alloys Compd.*, 2020, **819**, p 152962.
36. W. Ma, Y. Xi, C. Chen, H. Fukanuma, J. Wang, Z. Ren and R. Huang, Microstructural and Mechanical Properties of High-Performance Inconel 718 Alloy by Cold Spraying, *J. Alloys Compd.*, 2019, **792**, p 456-467.
37. S. Yin, W. Li, B. Song, X. Yan, M. Kuang, Y. Xu, K. Wen and R. Lupoi, Deposition of FeCoNiCrMn High Entropy Alloy (HEA) Coating via Cold Spraying, *J. Mater. Sci. Technol.*, 2019, **35**(6), p 1003-1007.
38. S. Yin, J. Cizek, C. Chen, R. Jenkins, G. O'Donnell and R. Lupoi, Metallurgical Bonding between Metal Matrix and Core-Shelled Reinforcements in Cold Sprayed Composite Coating, *Scr. Mater.*, 2020, **177**, p 49-53.
39. S. Yin, Y. Xie, J. Cizek, E.J. Ekoi, T. Hussain, D.P. Dowling and R. Lupoi, Advanced Diamond-Reinforced Metal Matrix Composites via Cold Spray: Properties and Deposition Mechanism, *Compos. Part B Eng.*, 2017, **113**, p 44-54.
40. R. Huang and H. Fukanuma, Study of the Influence of Particle Velocity on Adhesive Strength of Cold Spray Deposits, *J. Therm. Spray Technol.*, 2012, **21**, p 541-549.
41. J.R. Hönnige, P. Colegrove and S. Williams, Improvement of Microstructure and Mechanical Properties in Wire + Arc Additively Manufactured Ti-6Al-4V with Machine Hammer Peening, *Procedia Eng.*, 2017, **216**, p 8-17.

**Publisher's Note** Springer Nature remains neutral with regard to jurisdictional claims in published maps and institutional affiliations.